Two-pulse control over double ionization pathways in CO2

Sonia Erattupuzha, Seyedreza Larimian, Andrius Baltuška, Xinhua Xie, and Markus Kitzler

Citation: The Journal of Chemical Physics **144**, 024306 (2016); doi: 10.1063/1.4939638
View online: http://dx.doi.org/10.1063/1.4939638
View Table of Contents: http://scitation.aip.org/content/aip/journal/jcp/144/2?ver=pdfcov
Published by the AIP Publishing

Two-pulse control over double ionization pathways in CO_2

Sonia Erattupuzha, Seyedreza Larimian, Andrius Baltuška, Xinhua Xie, and Markus Kitzler[a)]
Photonics Institute, Vienna University of Technology, Gusshausstrasse 27, A-1040 Vienna, Austria

(Received 30 October 2015; accepted 23 December 2015; published online 12 January 2016)

We visualize and control molecular dynamics taking place on intermediately populated states during different sequential double ionization pathways of CO_2 using a sequence of two delayed laser pulses which exhibit different peak intensities. Measured yields of CO_2^{2+} and of fragment pairs CO^+/O^+ as a function of delay between the two pulses are weakly modulated by various vibronic dynamics taking place in CO_2^+. By Fourier analysis of the modulations we identify the dynamics and show that they can be assigned to merely two double ionization pathways. We demonstrate that by reversing the sequence of the two pulses it becomes possible to control the pathway which is taken across CO_2^+ towards the final state in CO_2^{2+}. A comparison between the yields of CO_2^{2+} and CO^+/O^+ reveals that the modulating vibronic dynamics oscillate out-of-phase with each other, thus opening up opportunities for strong-field fragmentation control on extended time scales. [http://dx.doi.org/10.1063/1.4939638]

I. INTRODUCTION

When a molecule interacts with a strong laser field multiple ionization, i.e., the loss of two or more electrons, may take place.[1] Depending on whether the electrons are removed from the outermost or from lower lying valence shells during this process, the molecular ion will be created in the ground or excited ionic states, respectively. The latter are often dissociative. Thus, by selective removal of electrons from either inner or outer valence orbitals the fragmentation of molecules can be controlled. This idea has been successfully implemented in experiments exploiting the dependence of the electron-recollision energy on the carrier-envelope phase,[2] the different ionization rates from inner, respectively, outer valence orbitals due to their different shapes[3] and their different sensitivity to laser intensity[4] and pulse duration.[5]

In a multiple ionization process, the final molecular ionic state may be reached via different pathways along intermediately populated ionic potential energy surfaces.[4] Between each ionization step nuclear restructuring may take place on the ionic potential energy surface(s) populated during the previous ionization event. The further fate of the molecule and therewith the outcome of a molecular fragmentation reaction depend on the history of all electron removal processes and on the delay between successive ionization steps. For example, it was recently shown for triple ionization of ethylene with laser pulses of different durations that a small increase in the delay between the second and third ionization steps determines whether the trication dominantly fragments into two, respectively, three moieties.[5] This behaviour could be explained to be due to the further stretch of the C–H bonds in the dication during this additional time.

Here, we report on experiments that generalize this concept to arbitrary delays between two ionization events. Using double ionization of CO_2 as an example, we show experimentally that two independent ionization events driven by a sequence of two ultrashort laser pulses with different intensity and an adjustable delay between them can be employed to control the pathway towards the final state in the doubly charged molecular ion. The different state transitions within the molecule which are triggered by the two ionization events are depicted by light- and dark-blue arrows in the energy level diagram in Fig. 1. We demonstrate that by reversing the sequence of the two pulses it becomes possible to control the pathway which is taken across different intermediately populated states in CO_2^+ towards the final state in CO_2^{2+} [X vs. A in Fig. 1]. A weaker (stronger) first pulse results in dominant ionization from the most weakly (more strongly) bound valence levels and therewith into population of different states in the cation (red-shaded energy region in Fig. 1). As a result, different electronic and vibrational dynamics are triggered on the different potential energy curves of CO_2^+. We show that by scanning the delay, Δt, between the two pulses, we can map these dynamics which take place on the intermediately populated states in CO_2^+ at times $t = \Delta t$, exemplarily shown in Fig. 1 for the symmetric C–O stretch motion $R_{CO}(t)$.

II. EXPERIMENT

In our experiments a sequence of two relatively delayed 25 fs (FWHM) laser pulses from a Titanium-Sapphire laser amplifier system is generated using a Mach-Zehnder interferometer with two 50:50 broad-band beam splitters and a position-controlled piezo-stage for varying the delay in steps of 4 fs. The pulse energy in one of the arms was decreased by reflecting off a portion of the beam

a)Electronic mail: markus.kitzler@tuwien.ac.at

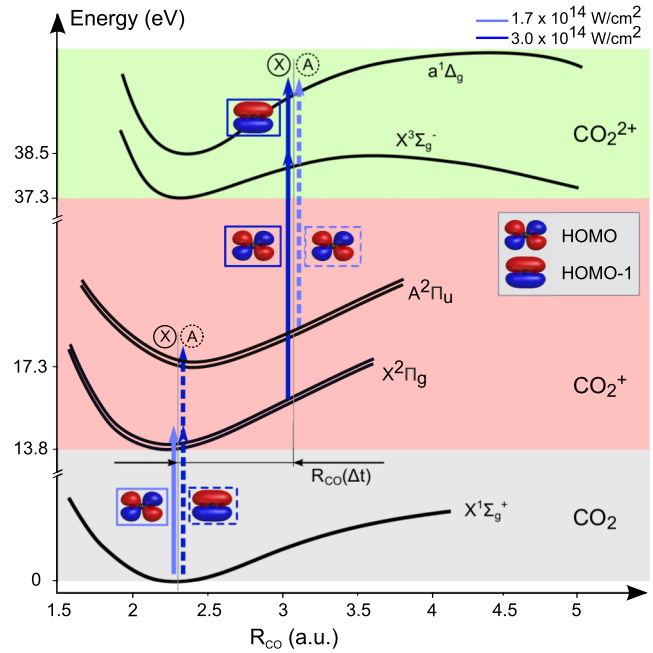

FIG. 1. Schematics of selected energy levels of CO_2, CO_2^+, and CO_2^{2+}. The energy curves for CO_2 and CO_2^+ are shown over C–O distance for the symmetric stretch vibrational mode. The energy curves for CO_2^{2+}, adapted from Ref. 13, are shown for the distance between CO^+ and O^+. The curves of the cation and neutral are taken from Ref. 14. To obtain a correct scaling of these curves over C–O distance they were stretched by preserving their relative sizes such that the neutral ground state matched the one in Ref. 15. Vertical arrows depict transitions due to removal of an electron from either HOMO or HOMO-1 (as indicated by shape, see legend). Light/dark color indicates ionization by the weaker/stronger pulse, and full and dashed arrows indicate the two pathways X and A, which are labelled after the state in CO_2^+ that is populated by the first ionization event. See text for further details.

using a pellicle under grazing incidence. The two beams are then focussed collinearly in an ultra-high vacuum chamber ($\sim 1 \times 10^{-10}$ mbar) of a reaction microscope[6,7] onto a supersonic gas jet of CO_2 molecules using a spherical silver mirror with a focal length of 60 mm. The polarization directions of the two linearly polarized beams were parallel to the spectrometer axis. Details on the experimental setup can be found in our previous publications.[2,8,9]

Ions resulting from the interaction of one CO_2 molecule with a sequence of two pulses were guided to a time and position sensitive channel plate detector by a weak homogeneous electric field (10.5 V/cm). From all ions detected in coincidence the three-dimensional momentum vectors were calculated. Molecular fragmentation channels were selected during the off-line data analysis by applying momentum conservation conditions in all three dimensions. The peak intensities of the pulses were estimated from the shape of the time-of-flight spectrum of H_2 dissociation[10] measured for each laser beam separately and were found to be 1.7×10^{14} and 3×10^{14} W/cm^2 for the weaker and stronger pulse, respectively. Such obtained intensities were found in good agreement with those estimated from the $2\sqrt{U_p}$ cut-off momentum of electrons released by field-ionization.[11,12] The spectral cutoff was evaluated directly in the momentum distribution of the CO_2^+ ions, which is possible because of momentum conservation between the electron and the ion.

III. RESULTS AND DISCUSSION

A. Modulation of ionization and fragmentation yield by molecular dynamics

Fig. 2(a) shows the measured yield of CO_2^+ and CO_2^{2+}, as well as the yield of the fragmentation channel CO^+/O^+ as a function of the delay between the pulses in the range of

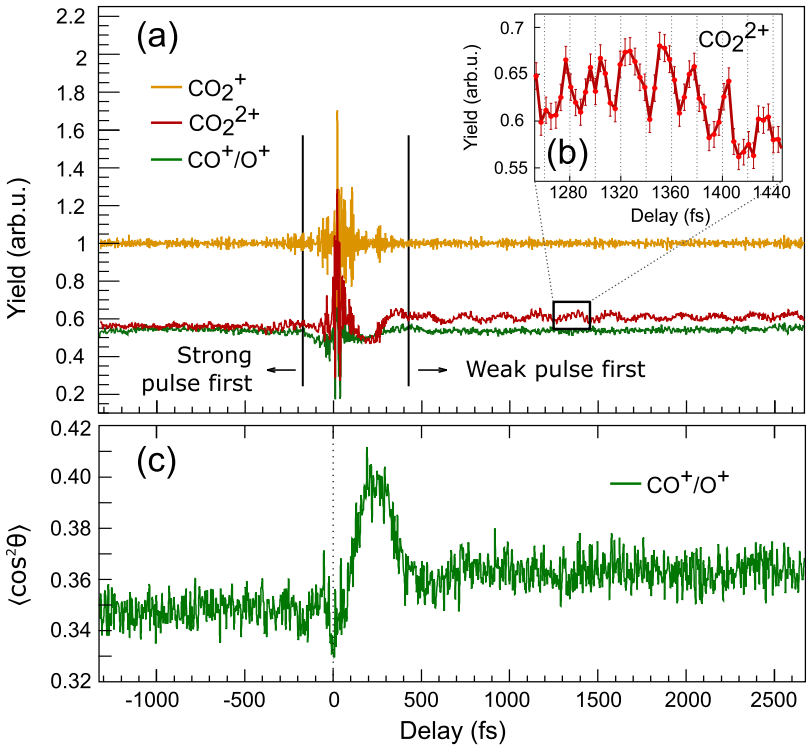

FIG. 2. (a) Measured yield of CO_2^+, CO_2^{2+}, and CO^+/O^+ as a function of the delay between the two pulses. (b) Zoom into a short delay-range of the CO_2^{2+}-yield with statistical error bars added. (c) Delay-dependence of the molecular alignment parameter $\langle \cos^2\theta \rangle$ calculated from the momentum vectors of the fragment ion pair CO^+/O^+.

$\Delta t = -1.3 \cdots + 2.6$ ps, where negative delays mean that the stronger pulse arrives earlier. The yields are normalized to the one of CO_2^+ at large delays. The measured traces of the ionization and fragmentation yields exhibit several interesting signatures on top of the dominant delay-independent signals that are mostly caused by the stronger of the two pulses. It can be seen that the yields are weakly modulated with various frequencies that are different for positive and negative delays. This is exemplified by the zoom into the yield of CO_2^{2+} shown in Fig. 2(b). In the delay region around $\Delta t = 0$, where the two pulses overlap, the ionization and fragmentation yields exhibit very strong modulations due to field-extinction and -enhancement effects.

At $\Delta t \approx 250$ fs one can see a pronounced dip in the CO_2^{2+} yield. This dip is attributed to the prompt feature in the creation of a rotational wave packet in CO_2 and CO_2^+ upon interaction with the weak first laser pulse.[16–18] Owing to the dependence of the ionization yield on the alignment of the molecule relative to the laser field direction this leads to a variation in the yield.[19–21] To prove that this dip is caused by the molecular alignment, we calculated the alignment parameter $\langle \cos^2\theta \rangle$ from the momentum vectors of the fragment ion pair CO^+/O^+, plotted in Fig. 2(c) over the delay. In perfect agreement with the dip in the CO_2^{2+} signal, the value of $\langle \cos^2\theta \rangle$ increases shortly after the application of the weak pulse at $\Delta t = 0$. It reaches its peak value at the same delay where also the CO_2^{2+} yield minimizes and subsequently decreases synchronously with the rise of the CO_2^{2+}-yield. Owing to the angular dependence of the ionization probability of CO_2, which shows a minimum for molecules aligned parallel with the laser polarization direction,[19] the CO_2^{2+}-yield decreases with increasing $\langle \cos^2\theta \rangle$, for which the molecules exhibit smaller angles with the laser polarization direction of the probe pulse.

After the prompt alignment feature, both the CO_2^{2+}-yield and the $\langle \cos^2\theta \rangle$ stay at a higher value than before the application of the weak pump pulse. This can be explained by the selection rules for Raman transitions between the rotational states that are driven by the weak pulse and which are the cause of the molecular alignment. These dictate a net increase in J-values and therewith lead to a delay-independent net alignment.[22] This net alignment is the reason why the CO_2^{2+} signal stays at a higher average value for $\Delta t > 500$ fs.

With a rotational constant of 0.39 cm^{-1} for the neutral molecule,[23] the created rotational wave packet is expected to revive after about 42 ps. As a consequence, even the quarter-revival is far outside the range of maximum delay of 2.6 ps set in our experiment and we therefore should not expect to see any signs of this rotational wave packet except for that of the prompt feature. In the following, we will focus on the vibronic dynamics which take place on the intermediately populated potential energy surfaces in CO_2^+ under field-free conditions sufficiently long after the interaction with the first laser pulse as indicated by full vertical lines and arrows in Fig. 2.

B. Analysis of molecular dynamics in the frequency domain

To obtain insight into these electronic and nuclear dynamics, we analyzed the various weak modulations present in the yields in Fig. 2. To this end, we performed a Fourier analysis of the yields in Fig. 2(a) for $\Delta t < -200$ fs and $\Delta t > +500$ fs, respectively. The resulting spectra for CO_2^{2+} and CO^+/O^+ are shown in Figs. 3(a) and 3(b), respectively. With the given delay ranges the achieved spectral resolution is about 2.6 meV and 3.5 meV for positive and negative delays, respectively, for both the spectra corresponding to CO_2^{2+} and CO^+/O^+. The Fourier analysis of the CO_2^+-yield (not shown in Fig. 3) results in a spectrum with a single clear peak around 22 meV for positive delays. The Fourier spectra corresponding to the CO_2^{2+} and CO^+/O^+ signals in contrast contain several clearly visible peaks. The following features are apparent in the spectra in Fig. 3: (i) The position and strength of the peaks strongly depend on whether the strong or weak pulse interacts with the molecule first. (ii) Both the CO_2^{2+} and CO^+/O^+ signals contain the same Fourier components; however, the relative intensities of the peaks strongly differ. Because CO_2 is a molecule of importance for both terrestrial and astronomical physics, it has been thoroughly studied spectroscopically.[13,14,23–27] Therefore, the different spectral peaks that correspond to different vibronic dynamics in CO_2^+ can be well identified by comparison to the literature.

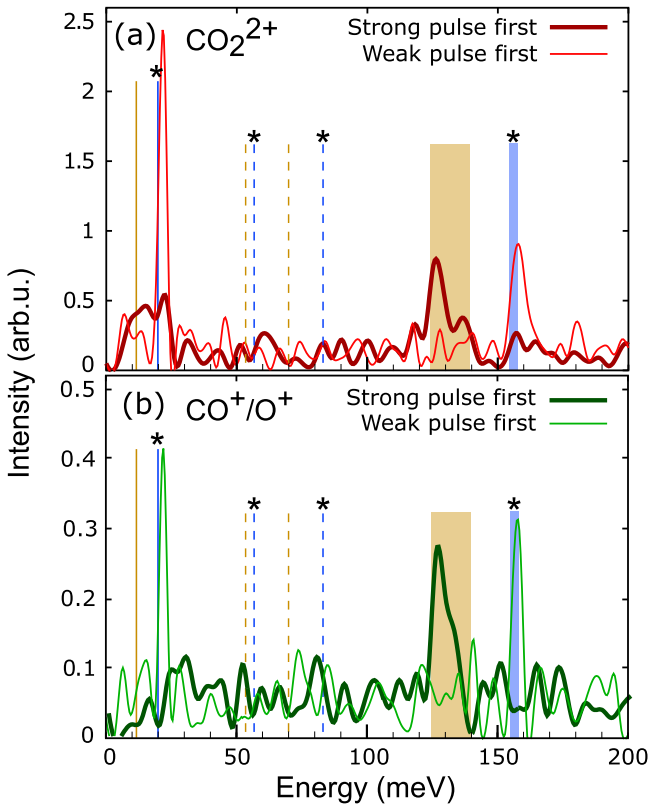

FIG. 3. Fourier transforms of the yield modulations from Fig. 2 for CO_2^{2+} (a) and CO^+/O^+ (b) for negative/positive pulse delays separately, encoded by thick/thin lines, respectively. The literature values[23–26] of electronic and vibrational transition energies of CO_2^+ are marked by lines and filled areas. Transitions on the X-state (A-state) are marked in blue (yellow) and with (without) an asterisk. Full and dashed lines indicate transitions due to electronic and bending dynamics, respectively. The range of transition energies corresponding to symmetric C–O stretch vibrational dynamics on both the X- and A-states is indicated by filled areas. See text for further details.

1. Weak pulse comes first

Let us start with the case where the weak pulse interacts first with CO_2 ($\Delta t > 0$). The spectrum corresponding to this case [thin line in Fig. 3(a)] consists of two prominent peaks, one at the low energy of 22 meV and the other one at 158 meV, corresponding to modulations in the CO_2^{2+} yield with a period of about 188 fs and 26 fs, respectively. The underlying oscillations are identified as vibronic dynamics on the ground state ($X^2\Pi_g$) of CO_2^+. The spectral peak resulting from the fast oscillation coincides with the band of transition energies corresponding to the symmetric C–O stretch vibrational motion, and the low-energy peak that results from the slower oscillation is attributed to beating dynamics between the two electronic states $X^2\Pi_{1/2g}$ and $X^2\Pi_{3/2g}$ that result from spin-orbit splitting of the doubly degenerate X-state.[24,26] The spectral peak at 22 meV in the CO_2^+ signal that was mentioned above may therefore be understood as pathway interferences in the ionization to the $X^2\Pi_{1/2g}$ and $X^2\Pi_{3/2g}$ states during the first and second laser pulse. The focus of the current study is, however, the double-ionization dynamics and we therefore do not further analyze the dynamics leading to the modulation in the CO_2^+-yield. Electron removal from CO_2 during the weak laser pulse, thus, results in the population of the $X^2\Pi_g$ state of CO_2^+, and the second, stronger pulse probes the dynamics taking place on this state at the time $t = \Delta t$ by ionization to CO_2^{2+}.

Since the $X^2\Pi_g$ state is the ground state of CO_2^+, the first electron must be removed from the HOMO of CO_2. During the second ionization event driven by the stronger pulse, electrons can also be removed from lower valence shells of CO_2^+. For reasons that will become clear below it is sufficient to consider electron removal from the HOMO and HOMO-1, which results in the population of the ground ($X^3\Sigma_g^-$) and first excited states ($a^1\Delta_g$) of CO_2^{2+}. Transitions between the ground and first excited state of CO_2^{2+} by photon-absorption after the preparation of CO_2^{2+} in its X-state can be neglected due to spin selection rules. Thus, only the two ionization steps are decisive for the molecular pathway. The such identified molecular pathway towards CO_2^{2+} via population of the X-state of CO_2^+ is denoted by X and indicated in Fig. 1.

2. Strong pulse comes first

The spectrum corresponding to the case where the strong pulse interacts first with the CO_2 molecule ($\Delta t < 0$) [thick line in Fig. 3(a)] is dominated by a spectral feature around 128 meV, corresponding to an oscillation period of 32 fs for the center frequency. This spectral feature largely overlaps with the band of transition energies corresponding to symmetric C–O stretch vibrations on the first excited state ($A^2\Pi_u$) of CO_2^+ indicated in Fig. 3(a).[24,25] The band indicated in the figure comprises the literature values of transition energies up to the 9th vibrational level of the electronic A-state.[25] The band arises because the vibrational transition energies become smaller for higher lying vibrational states and therefore the spectrum broadens towards smaller energies as higher vibrational levels are populated. The spectrum was arbitrarily terminated at the 9th vibrational level based on measured relative intensities.[25] When normalized to the first vibrational level the progressively decaying intensities stay above 10% up to the 5th and reach about 1% for the 9th vibrational level.

To prepare CO_2^+ on the A-state and to launch vibrational dynamics, the strong laser pulse must remove an electron from the HOMO-1 of CO_2. The subsequent weaker laser pulse then probes this dynamics on the CO_2^+ $A^2\Pi_u$ state and doubly ionizes the molecule by removing an electron from the HOMO of CO_2^+, thereby preparing CO_2^{2+} in its first excited a-state. This pathway for double ionization of the CO_2 molecule is marked with A in Fig. 1. The possibility of electron removal from the HOMO-1 of CO_2^+ by the weak pulse can be excluded because, on the one hand, the probability for this process is significantly decreased due to the stronger binding energy and the therewith reduced ionization rate.[1] More fundamentally, on the other hand this process would prepare CO_2^{2+} in an excited state beyond the a-state, which is incompatible with the observed fragmentation dynamics into CO^+/O^+, as will be explained below.

C. Dynamical origin of yield modulations and pathway selectivity

Modulations in the yield of CO_2^{2+} and CO^+/O^+ can, thus, be used for visualizing the ionization-induced molecular dynamics. We would like to note, however, that the yield is actually only the simplest quantity that can be analyzed in a coincidence momentum experiment. More advanced quantities such as angular distributions, or measures obtained by exploiting the correlation between different quantities that can be analyzed in experiments with better statistics than in our experiment, may lead to still deeper insight into the induced dynamics. The reason why already such a simple quantity, the yield of the final ionic products, is a sensitive measure for electronic beating and vibrational dynamics, is that the strong-field ionization probability sensitively depends on both molecular geometry and electronic structure.[3,19,28] In particular, the ionization rate is very sensitive to changes in the electronic structure along the laser polarization direction, as has been shown in experiments that probed the beating dynamics between two spin-orbit states in the Ne^+ ion.[28] The observed modulation of the CO_2^{2+} and CO^+/O^+ yields at the electronic beating frequency on the spin-orbit split X-state of CO_2^+ [Fig. 3] is attributed to such structure-induced changes in the ionization rate. Likewise, vibrational dynamics on both the X- and A-state of CO_2^+ leads to a change in the effective ionization potential, I_p, as the molecular geometry changes. For the symmetric stretch vibrational mode shown in Fig. 1, for both the X- and A-states the I_p increases on the order of 1-2 eV as the inter-nuclear distance stretches. This translates into a noticeable modulation of the ionization yield via the exponential dependence of the ionization rate on I_p.[1]

Changes in the effective ionization potential and therewith in the ion yield due to molecular restructuring dynamics can of course not only be induced by stretch vibrational modes. The effective I_p can change noticeably also for other types of vibrational restructuring dynamics, e.g., for bending

motion. However, as indicated in Fig. 3(a), the transitions corresponding to bending dynamics are at significantly lower energies than those of the symmetric stretch motion, and there is no overlap of any of them with peaks in the experimental data. The same is true for peaks corresponding to asymmetric stretch motion (not indicated in Fig. 3). Additionally, the Franck-Condon factors for populating levels corresponding to the symmetric stretch vibrational modes are by far the strongest ones.[25,26] Consequently, the dominant vibrational dynamics visible in the experimental data are the symmetric stretch vibrational modes on both the X- and A-state of CO_2^+ [cf. the peaks at 128 and 158 meV in Fig. 3(a)].

Turning to beating dynamics between electronic states, we note that the $A^2\Pi_u$ state of CO_2^+ that is populated by the strong pulse during pathway A is, like the X-state, doubly degenerate. The two spin-orbit split states $A^2\Pi_{1/2}u$ and $A^2\Pi_{3/2}u$ are separated by about 12 meV.[24–26] Therefore, one should expect that, similar to the observed beating dynamics on the X-state, the strong pump pulse should launch slow beating dynamics with a period of about 345 fs on them. However, the experimental data do not show a clearly resolved spectral peak in this energy range [cf. Fig. 3(a)]. A possibility for the absence of a clear peak may be that the beating between these states and the change in electronic structure due to it does not result in a pronounced enough modulation of the CO_2^{2+} yield and thus renders our experiment insensitive to beating between the $A^2\Pi_{1/2}u$ and $A^2\Pi_{3/2}u$ states.

Finally, we discuss the reason of the observed switching between pathways X and A depending on whether the strong or weak pulse comes first. When the weak pulse comes first, only dynamics on the X-state of CO_2^+ is launched and, as can be seen from the Fig. 3, no peaks corresponding to dynamics on the A-state are visible. To populate the A-state of CO_2^+, the weak pulse should remove an electron from the HOMO-1 of CO_2, which is by 3.5 eV more strongly bound than the HOMO. Due to the exponential dependence of the ionization rate on energy this additional binding energy leads to strongly suppressed ionization from the HOMO-1. Therefore, the A-state is not or only very weakly populated when the weak pulse comes first and the pathway marked by X in Fig. 1 becomes dominant.

In contrast, when the strong pulse comes first, Fig. 3(a) shows that the spectral peaks at 22 meV and 158 meV, corresponding to slow beating dynamics and symmetric stretch vibrational dynamics on the X-state of CO_2^+, respectively, are absent. Only dynamics on the A-state of CO_2^+ can be observed when the strong pulse comes first [cf. the peak around 128 meV], although the strong pulse most likely also causes ionization from the HOMO of CO_2 (and not only from the HOMO-1), which leads to population of the X-state of CO_2^+. However, the effective ionization potential for removing an electron from CO_2^+ in its X-state (into the X-state of CO_2^{2+}) is by approximately 2–3 eV higher than for ionization from the A-state (into the a-state of CO_2^{2+}). By virtue of the exponential energy dependence of the ionization rate this effectively suppresses this transition and the pathway marked by A in Fig. 1 becomes dominant when the strong pulse comes first.

IV. PATHWAY CONTROL OF CO^+/O^+ FRAGMENTATION DYNAMICS

The fact that the yield of the fragmentation products CO^+/O^+ shows almost identical spectral features (albeit with different relative intensities) and a very similar dependence on the pulse sequence as the CO_2^{2+}-yield [compare Figs. 3(a) and 3(b)], indicates that fragmentation reactions might also be amenable to pathway-control demonstrated for CO_2^{2+} above. In order to investigate this possibility we now turn to the molecular pathways leading to the fragmentation products CO^+/O^+.

We first note that both the ground ($X^3\Sigma_g^-$) and the first excited state ($a^1\Delta_g$) of CO_2^{2+} are meta-stable [cf. Fig. 1], and dissociation from either of the two states results in the moieties CO^+/O^+.[13] The a-state has, however, a significantly higher dissociation barrier than the X-state. Higher lying excited states also support the fragmentation reaction, but their dissociation barriers are still higher[13] and we therefore neglect them in our discussion. The kinetic energy release (KER) corresponding to fragmentation from the X-state of CO_2^{2+} into the moieties CO^+/O^+ predicted by simulations[13] ranges between approximately 5.2 eV and 6.2 eV, depending on the vibrational state(s) from which the molecular ion fragments. The lower value corresponds to fragmentation from the ground vibrational state via tunneling through the dissociation barrier, the higher value to dissociation just over the barrier. Due to the deeper potential of the a-state, the respective KER predictions[13] for fragmentation on this state range from 3.1 eV to 6.1 eV. However, as the dissociation probability rapidly decreases with the barrier width, very low KER values below roughly 4.5 eV are unlikely. The measured KER distribution [Fig. 4(a)] is quite symmetrically centered around 5.7 eV with a width of about 1.8 eV, independent whether the strong or the weak pulse drives the second ionization step. Thus, the measured KER values are consistent with both scenarios, dissociation from the X-state and the a-state of CO_2^{2+}. Comparison with the range of simulated KER-predictions indicates that the states are populated relatively high up in energy, i.e., far away from their potential minimum, such that the potential barriers can be overcome or tunneled through with significant probability.

A. Analysis of modulations in fragmentation yield

Based on the findings gained from the KER distributions, we now try to obtain insight into the molecular dynamics leading to CO^+/O^+-fragmentations. First of all we note that in our experiments we also observe fragmentation reactions into CO^+/O^+ when only the strong pulse is applied. The application of the additional weak pulse only slightly modulates the CO^+/O^+-yield, as is also reflected by the fact that the CO^+/O^+-yield in Fig. 2(a) is largely independent of the delay between the weak and the strong pulse. The weak modulations of the yield with delay become only apparent by the Fourier analysis presented in Fig. 3(b), where the contributions of the symmetric stretch vibrational motion on the X- and A-states of CO_2^+ are reflected by the two peaks at 158 meV and 128 meV, respectively.

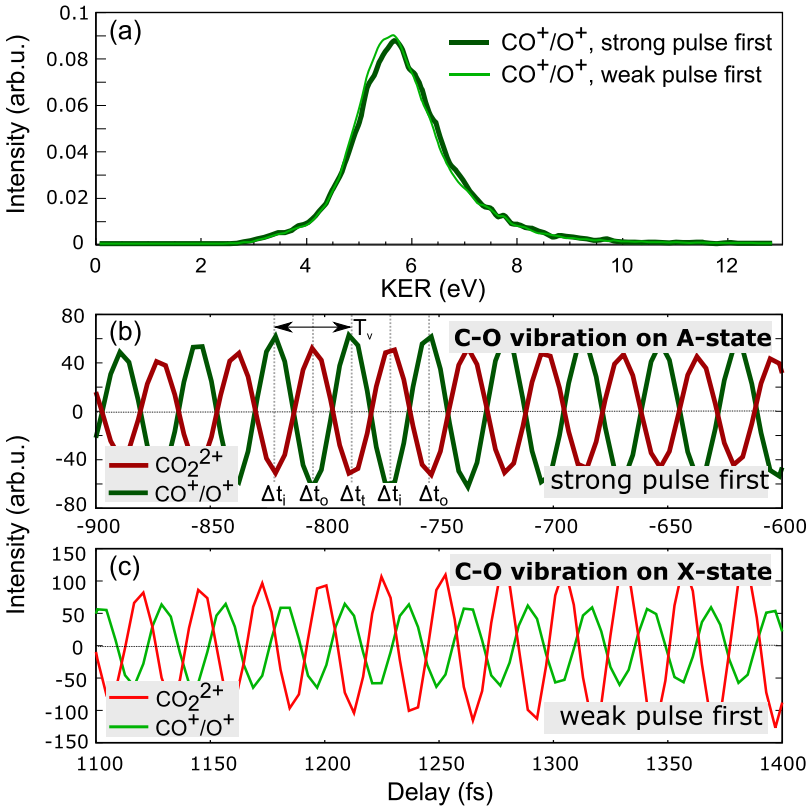

FIG. 4. (a) KER distribution of the fragments CO^+/O^+ for the two indicated cases. (b) Yield modulation of CO_2^{2+} and CO^+/O^+ over pulse delay obtained by inverse Fourier-transform of the signal contained in the peaks around 128 meV in Fig. 3 for the case when the strong pulse comes first. (c) Same as (b) but for the peaks around 158 meV when the weak pulse comes first. The labels Δt_i and Δt_o in (b) denote the pulse delays corresponding to the inner and outer turning points of the C–O vibrational motion. T_v indicates the full vibrational period of about 32 fs.

As mentioned, a noticeable influence of the stretch vibrational motion, i.e., a noticeable modulation amplitude on the CO^+/O^+-yield, necessitates that the X-state and particularly the significantly more strongly binding a-state of CO_2^{2+} are populated high up in energy. This is consistent with the conclusion made above that vibrational states up to the 9th level are populated during pathway A, for which fragmentation can only proceed via the more strongly binding a-state of CO_2^{2+} [cf. Fig. 1]. Population of high-lying vibrational states on the X- and a-states necessitates that in CO_2^+ the C–O bonds need to stretch far from their equilibrium distance, such that $|R_{CO} - R^e_{CO}|$, with R^e_{CO} the equilibrium C–O bond distance, becomes large. The shapes of the X- and a-state potential curves of CO_2^{2+} in Fig. 1 suggest that, for a given value of $|R_{CO} - R^e_{CO}|$, higher vibrational states and therefore higher dissociation probability, denoted by Γ_d in the following, are reached when CO_2^{2+} is populated at the inner rather than the outer turning points of the vibrational motion in CO_2^+. For the outer turning points Fig. 1 implies that the X- and a-state potential curves of CO_2^{2+} should be populated somewhat lower in energy, i.e., the dissociation probability should be smaller in these cases. The observed yield of fragment ions CO^+/O^+ as a function of delay is then determined by the product of Γ_d with the probability for ionization of CO_2^+ to CO_2^{2+}. The latter quantity is exponentially sensitive to the vertical energy difference between the different participating states in CO_2^+ and CO_2^{2+} and therewith depends strongly on R_{CO} and the exact shape of the potential curves. It is therefore difficult to intuitively predict the dependence of the yield of fragments CO^+/O^+ on R_{CO}.

B. Phase of yield-modulations

To gain insight into the dependence of ionization and dissociation on R_{CO} and the underlying vibrational dynamics, as well as on the branching of the molecular pathway into CO_2^{2+} or CO^+/O^+, we filtered out the separate peaks in Fig. 3 and performed phase-preserving inverse Fourier transforms for each of them. Sections of the resulting oscillations in the time-domain of the yields of CO_2^{2+} and CO^+/O^+ connected with the two high-energy peaks (symmetric C–O vibrations) on the A-state and X-state of CO_2^+ are shown in Figs. 4(b) and 4(c), respectively. It can be seen that for both pathways the yield of CO^+/O^+ is high when that of CO_2^{2+} is low and vice versa and that both yields peak only once per vibrational period, indicated in Fig. 4(b) with an arrow.

For pathway A [Fig. 4(b)] the yield modulations of CO^+/O^+ and CO_2^{2+} are exactly out of phase. This is also the case for the yield modulations caused by spin-orbit beating on the X-state (not shown in Fig. 4). These anti-cyclic yield modulations show that only one population event of the a-state of CO_2^{2+} per vibrational period leads to dissociation respectively production of stable CO_2^{2+}. Following from the discussions in Sec. III, we may assume that the population event that leads to dissociation takes place at the inner turning point of the vibrational motion, i.e., when R_{CO} minimizes. With that assumption our experiment shows that the dissociation probability at the outer turning point, reached half a vibrational period later or earlier, minimizes. As discussed above, this can be caused by a reduced dissociation probability due to population of the a-state at

lower energies. It follows that for this case the CO_2^{2+} ion should be produced with higher probability, which is indeed the case [cf. Fig. 4(b)]. In between the maxima and minima of the yields of CO_2^{2+} and CO^+/O^+ at the outer and inner turning points, both yields reach average values. In principle, the yield of CO_2^{2+} could also be expected to reach high values at delays where the vibrational motion is sampled around R_{CO}^e. A possible reason why this is not the case could be a smaller ionization probability at this molecular configuration.

The same picture is, in principle, applicable to the yield-oscillations observed for pathway X, in which the weak pulse comes first and C–O vibrational dynamics takes place on the X-state of the cation. In this case, however, the yields of CO_2^{2+} and CO^+/O^+ do not oscillate exactly out of phase [cf. Fig. 4(c)]. A small phase deviation of about 30° away from exactly out-of-phase is observed. The small deviation might be explained by the fact that for this pathway, in addition to the a-state, also the quite weakly binding X-state of CO_2^{2+} can be populated by the second ionization step. This opens up an additional possibility for dissociation and therewith might permit dissociation for a larger range of R_{CO} values. In addition, the potential energy curve of the X-state of CO_2^+ is notably more anharmonic than the one of the A-state and its minimum is situated towards smaller R_{CO} values [cf. Fig. 1], which leads to a different dependence of the vertical ionization potential on R_{CO} as compared to the A-state and therefore can also be the reason for the different phase-relation in the oscillations of the yields of CO_2^{2+} and CO^+/O^+.

Although the actual modulation depth of the yields over Δt is small [cf. Fig. 2], the fact that the probabilities for creating CO^+/O^+ respectively CO_2^{2+} peak at distinctively different Δt revealed by this analysis, thus, demonstrates that a double-pulse scheme provides selectivity for determining not only the pathways across intermediate molecular states but also for controlling the fragmentation behaviour of polyatomic molecules, therewith enhancing the flexibility of previously investigated single-pulse control schemes.[4,5]

V. SUMMARY

In summary, we have shown that sequential ionization with two delayed pulses that exhibit different, appropriately chosen peak intensities allows controlling the pathway across intermediately populated states in CO_2^+ and the dynamics taking place on these states. We demonstrated switching between two pathways by exchanging the sequence of the two laser pulses. The different molecular dynamics resulting from this were visualized in the yield-modulations of CO_2^{2+} and CO^+/O^+.

ACKNOWLEDGMENTS

We acknowledge financial support by the Austrian Science Fund (FWF) under Grant Nos. P28475-N27, P21463-N22, P25615-N27, P27491-N27, and SFB-F49 NEXTlite, and by a starting grant from the ERC (project CyFi).

[1]F. Krausz and M. Ivanov, Rev. Mod. Phys. **81**, 163 (2009).
[2]X. Xie, K. Doblhoff-Dier, S. Roither, M. S. Schöffler, D. Kartashov, H. Xu, T. Rathje, G. G. Paulus, A. Baltuška, S. Gräfe, and M. Kitzler, Phys. Rev. Lett. **109**, 243001 (2012).
[3]X. Xie, K. Doblhoff-Dier, H. Xu, S. Roither, M. S. Schöffler, D. Kartashov, S. Erattupuzha, T. Rathje, G. G. Paulus, K. Yamanouchi, A. Baltuška, S. Gräfe, and M. Kitzler, Phys. Rev. Lett. **112**, 163003 (2014).
[4]X. Xie, S. Roither, M. Schöffler, E. Lötstedt, D. Kartashov, L. Zhang, G. G. Paulus, A. Iwasaki, A. Baltuška, K. Yamanouchi, and M. Kitzler, Phys. Rev. X **4**, 021005 (2014).
[5]X. Xie, E. Lötstedt, S. Roither, M. Schöffler, D. Kartashov, K. Midorikawa, A. Baltuška, K. Yamanouchi, and M. Kitzler, Sci. Rep. **5**, 12877 (2015).
[6]R. Dörner, V. Mergel, O. Jagutzki, L. Spielberger, J. Ullrich, R. Moshammer, and H. Schmidt-Böcking, Phys. Rep. **330**, 95 (2000).
[7]J. Ullrich, R. Moshammer, A. Dorn, R. Dörner, L. P. H. Schmidt, and H. Schmidt-Böcking, Rep. Prog. Phys. **66**, 1463 (2003).
[8]L. Zhang, S. Roither, X. Xie, D. Kartashov, M. Schöffler, H. Xu, A. Iwasaki, S. Gräfe, T. Okino, K. Yamanouchi, A. Baltuska, and M. Kitzler, J. Phys. B **45**, 085603 (2012).
[9]X. Xie, S. Roither, D. Kartashov, E. Persson, D. Arbó, L. Zhang, S. Gräfe, M. Schöffler, J. Burgdörfer, A. Baltuška, and M. Kitzler, Phys. Rev. Lett. **108**, 193004 (2012).
[10]A. Alnaser, X. Tong, T. Osipov, S. Voss, C. Maharjan, B. Shan, Z. Chang, and C. Cocke, Phys. Rev. A **70**, 23413 (2004).
[11]F. Grasbon, G. Paulus, H. Walther, P. Villoresi, G. Sansone, S. Stagira, M. Nisoli, and S. De Silvestri, Phys. Rev. Lett. **91**, 173003 (2003).
[12]A. Rudenko, K. Zrost, C. D. Schröter, V. L. B. D. Jesus, B. Feuerstein, R. Moshammer, and J. Ullrich, J. Phys. B **37**, L407 (2004).
[13]M. Hochlaf, F. R. Bennett, G. Chambaud, and P. Rosmus, J. Phys. B **31**, 2163 (1998).
[14]T. Zimmermann, H. Köppel, and L. S. Cederbaum, J. Chem. Phys. **83**, 4697 (1985).
[15]G. Herzberg, *Electronic Spectra and Electronic Structure of Polyatomic Molecules* (Van Nostrand, New York, 1966).
[16]J. Ortigoso, M. Rodrguez, M. Gupta, and B. Friedrich, J. Chem. Phys. **110**, 3870 (1999).
[17]F. Rosca-Pruna and M. Vrakking, Phys. Rev. Lett. **87**, 153902 (2001).
[18]H. Stapelfeldt and T. Seideman, Rev. Mod. Phys. **75**, 543 (2003).
[19]D. Pavičić, K. Lee, D. Rayner, P. Corkum, and D. Villeneuve, Phys. Rev. Lett. **98**, 243001 (2007).
[20]S. Petretti, Y. V. Vanne, A. Saenz, and P. Decleva, Phys. Rev. Lett. **104**, 223001 (2010).
[21]P. Krause and H. B. Schlegel, J. Phys. Chem. Lett. **6**, 2140 (2015).
[22]I. Litvinyuk, K. Lee, P. Dooley, D. Rayner, D. Villeneuve, and P. Corkum, Phys. Rev. Lett. **90**, 233003 (2003).
[23]P. Linstrom and W. Mallard, NIST Chemistry WebBook, NIST Standard Reference Database Number 69, http://webbook.nist.gov/chemistry/.
[24]P. Baltzer, F. T. Chau, J. H. D. Eland, L. Karlsson, M. Lundqvist, J. Rostas, K. Y. Tam, H. Veenhuizen, and B. Wannberg, J. Chem. Phys. **104**, 8922 (1996).
[25]J. Liu, M. Hochlaf, and C. Y. Ng, J. Chem. Phys. **113**, 7988 (2000).
[26]J. Liu, W. Chen, C.-W. Hsu, M. Hochlaf, M. Evans, S. Stimson, and C. Y. Ng, J. Chem. Phys. **112**, 10767 (2000).
[27]A. E. Slattery, T. A. Field, M. Ahmad, R. I. Hall, J. Lambourne, F. Penent, P. Lablanquie, and J. H. D. Eland, J. Chem. Phys. **122**, 84317 (2005).
[28]A. Fleischer, H. Wörner, L. Arissian, L. Liu, M. Meckel, A. Rippert, R. Dörner, D. Villeneuve, P. Corkum, and A. Staudte, Phys. Rev. Lett. **107**, 113003 (2011).